

Investigating Sterile Neutrino Flux in the Solar Neutrino Data

Ankush *, Rishu Verma †, Gazal Sharma ‡ and B. C. Chauhan §

*Department of Physics & Astronomical Science,
School of Physical & Material Sciences,
Central University of Himachal Pradesh (CUHP), Dharamshala, Kangra (HP), India 176215*

Abstract

There are compelling evidences for the existence of a fourth degree of freedom of neutrinos i.e. sterile neutrino. In the recent studies the role of sterile component of neutrinos has been found to be crucial, not only in particle physics, but also in astrophysics and cosmology. This has been proposed to be one of the potential candidates of dark matter. In this work we investigate the updated solar neutrino data available from all the relevant experiments including Borexino and KamLAND solar phase in a model independent way, and obtain bounds on the sterile neutrino component present in the solar neutrino flux. The mystery of the missing neutrinos is further deepening as subsequent experiments are coming up with their results. The energy spectrum of solar neutrinos, as predicted by standard solar models, is seen by neutrino experiments at different parts as they are sensitive to various neutrino energy ranges. It is interesting to note that more than 98% of the calculated standard model solar neutrino flux lies below $1MeV$. Therefore, the study of low energy neutrinos can give us better understanding and the possibility to know about the presence of antineutrinos and sterile neutrinos components in solar neutrino flux. As such, this work becomes interesting as we include the data from medium energy ($\sim 1MeV$) experiments i.e. Borexino and KamLAND solar phase. In our study we retrieve the bounds existing in literature, and rather provide more stringent limits on sterile neutrino (ν_s) flux available in solar neutrino data.

1 Introduction

H. Bethe proposed that the thermonuclear reactions are responsible for energy generation inside the stars, and it was consequently established too. Sun, being the closest star to us, glows due to these thermonuclear fusion reactions, which also produce a huge amount of neutrinos leaving the solar core without any hinderance. To look for these neutrinos, the era of the solar neutrino experiments began in the late 1960's with the Homestake solar neutrino detector, which was headed by astrophysicists Raymond Davis, Jr. and his theoretician friend John N. Bahcall. The purpose of this experiment was to verify the fusion reactions that power the sun by measuring the resulting neutrino fluxes. Instead of confirming the predictions of the Standard Solar Model (SSM) it discovered a significant deficit of neutrinos as compared to the expected flux by SSM. This puzzle later was named as the Solar Neutrino Problem (SNP) [1], [2]. After a journey of about four decades a leading solution for the SNP was identified with the help of reactor experiment KamLAND [3] in Japan, which independently verified neutrino oscillations through Large Mixing Angle (LMA) [4] as the dominant solution using neutrinos from nearby reactors. Motivated by peculiar nature of neutrinos, a number of subsequent experiments

*ankush.bbau@gmail.com

†rishuvm274@gmail.com

‡gazzal.sharma555@gmail.com

§chauhan@associates.iucaa.in

were performed, which rather than solving the mystery of the missing neutrinos, deepened it further. It came to the light that more than 98% of the solar neutrino flux lies below 1MeV . The rare ${}^8\text{B}$ neutrino flux is the high energy tail of solar neutrinos for which statistically significant measurements have been made so far. As such, the explored part of the flux is just a tip of an iceberg, there could be more mysteries hidden deep inside the water. Along with LMA there might be some sub-dominant effect(s) also affecting the nature and dynamics of these so called ghost particles. Therefore, the study of low energy neutrino data can give us better understanding and the possibility to explore the presence of sterile neutrinos and other components in solar neutrino flux.

Neutrinos are special and have a unique status in the Standard Model (SM) in the sense that they are massless and interact solely through the weak interaction. They are left handed only, i.e. active and partner of a corresponding charged lepton in a weak isospin doublet. As such, there is no place for the right-handed neutrinos in the SM. Right-handed neutrinos, if they exist, would be weak isospin singlets, i.e. even no weak interactions. They would communicate with the other SM member neutrinos (left-handed active neutrinos) through mixing only. That is the reason, the right-handed neutrinos are called as inactive i.e. sterile. There are mounting evidences for existence of additional degrees of freedom (>3) of neutrinos, which indicate the existence of a new class of heavy and light sterile neutrinos, and possibility of their mixing with active ones [5], [6].

The Stanford group has done analysis of the available solar neutrino data [7] that provided increasing evidence that the neutrino flux from the sun is not constant but varies with well-known solar rotation periods. If such findings are confirmed ever in future, the need for an addition to the LMA solution will be obvious and will most likely rely on an interaction of the solar magnetic field with the neutrino magnetic moment. Since an SFP (Spin Flavour Precession) conversion to active antineutrinos is unlikely, this interaction is expected to produce a significant and time varying flux of sterile neutrinos [5], [8] and [9]. It has become evident that the mechanism of SFP to active antineutrinos in the sun is either absent or plays a subdominant role. In fact these active neutrinos would originate a sizeable $\bar{\nu}_e$ flux [10], whose upper bound has become stricter and corresponds to 0.028% of the ${}^8\text{B}$ neutrino flux.

In the light of latest data available from various solar neutrino experiments, like the Neutral Current Detectors (NCDs) phase of Sudbury Neutrino Observatory (SNO), SuperK-III, SuperK-IV, Borexino and KamLAND solar phase [11] -[16] for neutrinos of energy range $\sim 1\text{MeV}$, we derive, in a model independent way, bounds on the sterile neutrino component present in the solar neutrino flux. We update the limits on the sterile neutrinos (ν_s) flux and compare them with the previous results obtained using various SNO phase data and data from SuperKamiokande experiments. Various such analysis [17] -[21] have been done in the past, but our results included all the experimental data, in a way it is a global data analysis and obtained more constrained limits on the sterile neutrino flux as compared to the bounds existing in the literature. The degeneracy of SSM normalisation factor (f_B), and active neutrinos($\sin^2\alpha$) is updated and best fit values for various cases using χ^2 analysis are obtained.

In section (2) we provide the experimental details and the data available from all the solar neutrino experiments. In section (3) we discuss the theory starting from the master equations. Section (4) presents results and discussion of our work including the χ^2 -Fitting for different cases of various experiments and the conclusions are finally summarised in section (5).

2 Data from various Solar Neutrino Experiments

Kamiokande, a large water Cerenkov detector, was primarily designed to do search for proton decay. It was diverted to take data of solar neutrinos in the second phase i.e. Kamiokande-II during 1985, and provided a directional information of solar neutrinos demonstrating directly for the first time that the sun is a source of neutrinos. Via elastic scattering(ES) experiment this also discovered the atmospheric neutrinos anomaly and observed neutrino signals from the supernova 1987A. Super-Kamiokande (SK) was designed after overhauling the Kamiokande to do search for proton decay, studied solar and atmospheric neutrinos, and watched the supernovae in the Milky Way Galaxy. SK is a cylindrical 50kt water Cerenkov detector which observes high energy solar neutrinos via elastic scattering of electrons. The Super-Kamiokande experiment started taking data in April, 1996 and continued the observation

for five years within the running period referred to SK-I till the detector maintenance in July, 2001. The SK detector was rebuilt after an accident met with the half of the original PMT density in the inner detector and resumed observation from October, 2002, which is referred to the beginning of SK-II running period. The SK-II continued the measurements for three years and finished in October 2005 for the reconstruction work to put the PMT density back to the SK-I level. The detector restarted observation in June, 2006, which is referred to the SK-III period. The fourth phase of SK (SK-IV) start of in September of 2008, with new front-end electronics, QBEE (QTC Based Electronics with Ethernet) [22] for new data acquisition system.

The data obtained from Sudbury Neutrino Observatory (SNO) consists also of high energy end part of 8B solar neutrinos. The SNO, based in Canada, detects neutrinos via three reaction channels 1) charged-current interactions(CC) on deuterons, in which only electron neutrinos participate; 2) neutrino-electron elastic scattering (ES), which are dominated by contributions from electron neutrinos and 3) neutral-current (NC) disintegration of the deuteron by neutrinos, which has equal sensitivity to all active neutrino flavours. So far, the SNO has three stages/ phases of running. The first phase was with pure D_2O (heavy water) ran from November 1999 to May 2001. In the second phase to increase the neutron detection efficiency 2000 kg of NaCl salt was added to the target material D_2O . This SNO-II (Salt phase) ran from June 2001 to October 2003. The third and final stage of SNO phase used Neutral Current Detectors (NCDs), which was achieved by the removal of the salt and addition of 36 strings of 3He proportional counters to provide an independent detection of neutrons. This SNO-III (NCDs) phase ran from November 2004 to November 2006. As these three stages have very different systematic uncertainties for the detection of neutrons, that means the stages of the SNO (Phase -I,II,III) can be considered as three independent experiments in measuring the flux of 8B solar neutrinos flux with the neutral current reaction. It is further added that the second SNO phase of running a data set of 254.2 days with a $5.5MeV$ energy threshold, and in the third phase of running for 385.2 days of data with a $5MeV$ energy threshold are taken.

KamLAND (Kamioka Liquid Scintillating Anti-Neutrino Detector) is located in the Kamioka Mine near the city of Kamioka in the Gifu prefecture of Japan. The reactor experiment KamLAND is exactly located in the old Kamiokande site within the mine. KamLAND started data collection in January 2002 and the results were reported using only 145 days of data. The detector consists of a 1000 metric tons (1 kilo-ton or 1kt) of liquid scintillator, as both the target and detection medium for low energy nuclear/particle physics processes like neutrino elastic scattering and inverse beta decay. The liquid scintillator molecules give off light when charged particle move through the detector. As such, the KamLAND is designed and instrumented to detect this light and reconstruct the physics processes that produce the light. In the solar phase KamLAND is focussed to detect medium energy solar neutrinos($\sim 1MeV$). We have taken the latest data for 8B solar neutrinos based on a 123 kton-day exposure of KamLAND [16]. KamLAND also reported measurement of the neutrino-electron elastic scattering rate $862\ keV\ ^7Be$ solar neutrino based on a 165.4 kton-days exposure of KamLAND for 616 days between April 7, 2009 and June 21, 2011 [23].

Borexino is an ultra-high radio purity detector located in the underground laboratory at Gran Sasso, Italy. It is a low threshold liquid scintillator detector, which detects solar neutrinos of medium energy range (7Be , CNO, pep) via elastic scattering of electrons. This detector is the first experiment able to do a real-time analysis of low energy sector solar neutrinos. The modelling of the detector response has been steadily improved since the beginning of data taking in 2007, and invaluable information has been provided by an extensive calibration campaign in 2009. As a target, 300t of liquid scintillator is contained in a spherical nylon vessel. To provide a passive shielding a non-scintillating buffer liquid is used outside. More than 2200 PMTs are mounted on the inner surface of a stainless steel sphere to register the scintillation light. The water volume shields the detector against external gamma and neutron radiations, which acts as an active muon veto.

Borexino reports the interaction rate of the $0.862\ MeV\ ^7Be$ solar neutrinos for 192 live days data in the period from May 16, 2007 to April, 12, 2008 (Borexino Phase-I). The first simultaneous measurement of the interaction rates of pp, 7Be , and pep solar neutrinos was taken in an extended energy range (0.19-2.93)MeV. This result pertains to the span of 1291.51days, i.e. Borexino Phase-II data, which was collected between December 2011 and May 2016 after an extensive scintillator purification campaign.

Borexino is the first experiment to succeed in suppressing all major backgrounds, above the 2.614MeV γ from the decay of ^{208}Tl , to a rate below that of electron scatterings from solar neutrinos. This allows to reduce the energy threshold for scattered electrons by ^8B solar neutrinos to 3MeV (Borexino(3MeV)). Borexino also reported the ^8B interaction rate with 5MeV threshold (Borexino(5MeV)).

Below the SNO-I, II, III and SK-I, SK-II, SK-III, SK-IV and Combined data from Superkamiokande experiment, KamLAND Solar Phase and Borexino(3MeV) and Borexino(5MeV) data are shown in the Table (1). In Table (2) survival probabilities of ^7Be solar neutrinos from KamLAND, Borexino Phase-I, Borexino Phase-II are given. In Table (3) we present the data in terms of the corresponding rates with reference to the SSM flux [24].

Data	ϕ^{CC}	ϕ^{NC}	ϕ^{ES}	Reference
SNO-I	1.76 ± 0.11	5.09 ± 0.45	2.39 ± 0.27	[11]
SNO-II	1.68 ± 0.10	4.94 ± 0.41	2.35 ± 0.27	[11]
SNO-III	1.67 ± 0.09	5.54 ± 0.47	1.77 ± 0.24	[11]
SK-I	-	-	2.38 ± 0.08	[13]
SK-II	-	-	2.41 ± 0.17	[13]
SK-III	-	-	2.40 ± 0.07	[13]
SK-IV	-	-	2.308 ± 0.044	[13]
SK Combined	-	-	2.345 ± 0.04	[13]
KamLAND	-	-	2.77 ± 0.41	[16]
Borexino(3MeV)	-	-	2.55 ± 0.20	[14]
Borexino(5MeV)	-	-	2.70 ± 0.45	[15]

Table 1: Solar Neutrino Flux measured by various experiments in units of $10^6\text{cm}^{-2}\text{s}^{-1}$.

Experiment	P_{ee}	Reference
KamLAND	0.66 ± 0.15	[23]
Borexino Phase-I	0.51 ± 0.07	[15]
Borexino Phase-II	0.53 ± 0.05	[25]

Table 2: Solar Neutrino Survival Probability measured by various experiments for ^7Be neutrinos.

Experiment	R^{CC}	R^{NC}	R^{ES}
SNO I	0.32 ± 0.04	0.93 ± 0.14	0.44 ± 0.07
SNO II	0.31 ± 0.04	0.90 ± 0.13	0.43 ± 0.07
SNO III	0.30 ± 0.04	1.01 ± 0.15	0.32 ± 0.05
SK I	-	-	0.43 ± 0.05
SK II	-	-	0.44 ± 0.06
SK III	-	-	0.44 ± 0.05
SK IV	-	-	0.42 ± 0.05
SK Combined	-	-	0.42 ± 0.05
KamLAND	-	-	0.51 ± 0.09
Borexino(3MeV)	-	-	0.46 ± 0.06
Borexino(5MeV)	-	-	0.49 ± 0.10

Table 3: Different rates with errors for the SNO, SK, KamLAND and Borexino experiments.

3 Model Independent Analysis Theory

In the master equations of the model independent analysis given below we have neglected electronic antineutrino component [21]

$$\phi^{CC} = \phi_{\nu_e}, \quad (1)$$

$$\phi^{NC} = \phi_{\nu_e} + \phi_{\nu_x} + \bar{r}_d \phi_{\bar{\nu}_x}, \quad (2)$$

$$\phi^{ES} = \phi_{\nu_e} + r \phi_{\nu_x} + \bar{r}_x \phi_{\bar{\nu}_x}. \quad (3)$$

From these equations we can see that the neutral current (NC) is sensitive equally for all neutrino components, the elastic scattering (ES) is more sensitive to electronic neutrino component than the non-electronic ones, and the charged current (CC) is only due to the electronic component of the neutrinos. We neglect the electronic antineutrino solar neutrino flux as evident from KamLAND results [10].

The quantities r , \bar{r}_x used are the ratios of the NC neutrino and non-electronic antineutrino event rates to the NC+CC neutrino event rate, respectively. The remaining \bar{r}_d is the ratio of the antineutrino deuteron fission to neutrino deuteron fission event rate. We calculated them using the following forms of expressions

$$r = \frac{\int dE_\nu \phi(E_\nu) \int dE_e \int dE'_e \frac{d\sigma_{NC}}{dE_e} f(E'_e, E_e)}{\sigma_{NC} \rightarrow \sigma_{NC+CC}}, \quad (4)$$

$$\bar{r}_x = \frac{\int dE_\nu \phi(E_\nu) \int dE_e \int dE'_e \frac{d\bar{\sigma}_{NC}}{dE_e} f(E'_e, E_e)}{\sigma_{NC} \rightarrow \bar{\sigma}_{NC+CC}}, \quad (5)$$

$$\bar{r}_d = \frac{\int dE_\nu \phi(E_\nu) \bar{\sigma}_{NC}(E_\nu)}{\bar{\sigma}_{NC} \rightarrow \sigma_{NC}}. \quad (6)$$

Here the energy resolution function is $f(E'_e, E_e)$ and σ 's are the cross sections. The subscript x in ν_x and $\bar{\nu}_x$ stands for the non-electronic (μ/τ) components. One can extract the expression for ES flux from the master equations (1)-(3) as

$$\phi^{ES} = r \phi^{NC} + (1-r) \phi^{CC} - (r \bar{r}_d - \bar{r}_x) \phi_{\bar{\nu}_x}. \quad (7)$$

If we neglect the antineutrino component, as there are stringent limits from KamLAND, the expression for ES flux is obtained as

$$\phi_{no\bar{\nu}_x}^{ES} = r \phi^{NC} + (1-r) \phi^{CC}. \quad (8)$$

Since we are specifically interested in estimating the flux of sterile neutrinos, therefore we derive an expressions for the active neutrino ($\nu_e + \nu_x + \bar{\nu}_x$), non-electronic neutrino component (ν_x) and thereafter the sterile neutrino ($\nu_{sterile}$) fluxes can be estimated as

$$\phi_{active} = \frac{[(r - \bar{r}_x) \phi^{NC} + (1 - \bar{r}_d)((1-r) \phi^{CC} - \phi^{ES})]}{r \bar{r}_d - \bar{r}_x}, \quad (9)$$

$$\phi_{\nu_x}^{NC} = \phi^{NC} - \phi^{CC}, \quad (10)$$

$$\phi_{\nu_x}^{ES} = \frac{\phi_{SK}^{ES} - \phi^{CC}}{r}. \quad (11)$$

We can get the expression for the sterile neutrino flux if we subtract the active neutrino flux from the SSM predictions as

$$\phi_{sterile} = \phi_{SSM}^B - \phi_{active}. \quad (12)$$

The active-sterile admixture can also be estimated as the mixing angle α between the active and sterile neutrinos, such that $\sin^2 \alpha$ will denote the fraction of the all the active neutrinos. Therefore the component of the sterile neutrinos is proportional to $\cos^2 \alpha$. Excluding the electronic component

the fraction of active neutrino flux, as measured by CC flux, present in the solar neutrino flux can be calculated by the following relation

$$\sin^2 \alpha = \frac{\phi_{active} - \phi^{CC}}{\phi_{SSM} - \phi^{CC}}. \quad (13)$$

The degeneracy between the sterile neutrino component and the parameter designated as f_B , the normalisation to the SSM 8B neutrino flux [24], can be clearly seen if we rewrite the model independent flux equations in terms of the expressions for the charged current(CC), neutral current(NC) and elastic scattering(ES) rates [20]

$$R^{CC} = f_B P_{ee}, \quad (14)$$

$$R^{NC} = f_B P_{ee} + f_B(1 - P_{ee})[\sin^2 \alpha \sin^2 \psi + \bar{r}_d \sin^2 \alpha \cos^2 \psi], \quad (15)$$

$$R^{ES} = f_B P_{ee} + f_B(1 - P_{ee})[r \sin^2 \alpha \sin^2 \psi + \bar{r}_x \sin^2 \alpha \cos^2 \psi]. \quad (16)$$

As evident from above equations, these are reduced rates. Here we exploit the near energy independence in the range of interest and factorize the electron neutrino survival probability P_{ee} out of these integrals as in equations (14)- (16). It is evident from the above equations that the electron neutrinos converted into the other flavours are proportional to $1 - P_{ee}$. Here $\sin^2 \psi$ gives the measure of antineutrino components.

Re-arranging the rate equations we get $\sin^2 \alpha$ and f_B degeneracy equation as

$$\sin^2 \alpha = \frac{R^{ES} - R^{CC}}{(f_B - R^{CC})r}. \quad (17)$$

Using ES rate equation and the survival probability P_{ee}^M for intermediate energy neutrinos, we obtain

$$R^{ES} = P_{ee}^M + (1 - P_{ee}^M)[r \sin^2 \alpha \sin^2 \psi + \bar{r}_x \sin^2 \alpha \cos^2 \psi], \quad (18)$$

where r and \bar{r}_x are cross-sectional ratios as defined above. From the above equation, rate for no antineutrino component ($\sin^2 \psi = 1$) and a sterile admixture with the active neutrinos is given as

$$R_{BOR/KL}^{ES} = P_{ee}^M + (1 - P_{ee}^M)r \sin^2 \alpha. \quad (19)$$

In both the cases the value of cross-sectional ratios r will be different.

As of today we know the corresponding ES rates (R_{BOR}^{ES} and R_{KL}^{ES}) and the survival probabilities for medium energy neutrinos (P_{ee}^M) from the experiments, therefore using these we can estimate the sterile neutrino flux component present in the observed data.

4 Results and Discussions

The standard solar model predictions [24] for 8B solar neutrino flux to be observed at all experiments is taken to be $\phi_{SSM} = 5.46 \pm 0.65 \times 10^6 \text{ cm}^{-2}\text{s}^{-1}$. We can have a number of possible combinations for our analysis, but we used only the ones, which were giving us the most constrained limits. So, we do our analysis for the Sets in which we use fluxes ϕ^{NC} , ϕ^{CC} from SNO-III with ϕ^{ES} from SNO-III, SK Combined, KamLAND, Borexino(3MeV), Borexino(5MeV) and flux of ϕ^{ES} common to all experiments as shown in Figure(1). We take all experiments one by one and derive constraints on f_B , active and sterile neutrinos. These Sets are shown in Table (4).

Set	ϕ^{CC}	ϕ^{NC}	ϕ^{ES}
1.	SNO-III	SNO-III	SNO-III
2.	SNO-III	SNO-III	SK Combined
3.	SNO-III	SNO-III	KamLAND
4.	SNO-III	SNO-III	Borexino(3MeV)
5.	SNO-III	SNO-III	Borexino(5MeV)
6.	SNO-III	SNO-III	ϕ^{ES} Overlap

Table 4: Grouping of data in different sets.

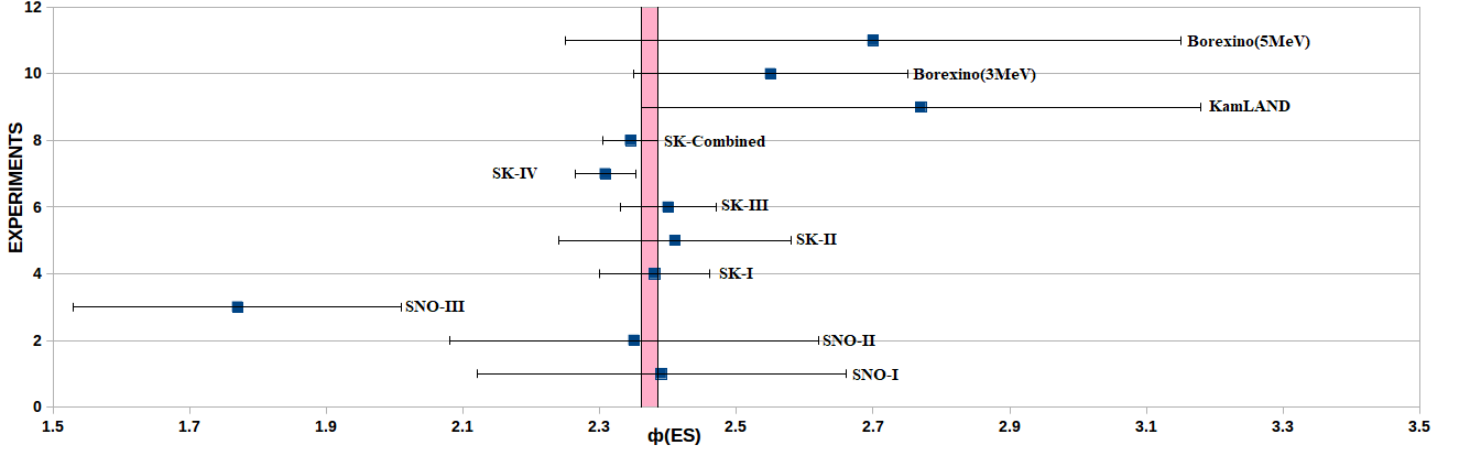


Figure 1: ϕ^{ES} Overlap region (shaded) from all experiments.

We use the equations (9), (12) and (13) and obtain the results as shown in Table (6). It is noted that, for no-sterile neutrinos, the CC/NC flux ratio in SNO is a direct measure of the average survival probability of 8B solar neutrinos that were detected through experiment as $P_{ee} = \phi^{CC}/\phi^{NC}$. Solving it with errors, we will have $P_{ee} = 0.306 \pm 0.04$ with SSM and $P_{ee} = 0.301 \pm 0.03$ with NC for high energy neutrinos. The difference in above two results for NC and SSM flux indicates the possibility for sterile neutrino flux present in the solar neutrino flux. The values of r , \bar{r}_x , \bar{r}_d used are shown in Table (5)

Experiment	r	\bar{r}_x	\bar{r}_d
SNO-I	0.150	0.115	0.954
SNO-II	0.150	0.115	0.954
SNO-III	0.151	0.116	0.955
SK-I	0.149	0.114	-
SK-II	0.151	0.116	-
SK-III	0.151	0.116	-
SK-IV	0.151	0.116	-
SK-Combined	0.151	0.116	-
KamLAND	0.210	-	-
Borexino(3MeV)	0.213	0.181	-
Borexino(5MeV)	0.213	0.181	-

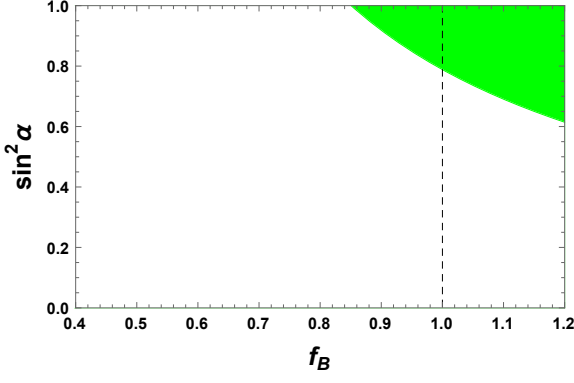
Table 5: Cross-sectional ratios for various experiments .

Set	Data Set	ϕ_{active}	$\phi_{sterile}$	$\sin^2\alpha$	Sterile %
1.	SNO-III	6.313 ± 0.708	-0.853 ± 0.961	1.225 ± 0.281	0 - 05.6
2.	SK Combined	5.395 ± 0.599	0.065 ± 0.884	0.983 ± 0.231	0 - 24.8
3.	KamLAND	4.879 ± 1.185	0.581 ± 1.352	0.847 ± 0.345	0 - 49.8
4.	Borexino(3MeV)	5.428 ± 0.794	0.032 ± 1.026	0.991 ± 0.269	0 - 27.8
5.	Borexino(5MeV)	5.127 ± 1.134	0.333 ± 1.307	0.912 ± 0.338	0 - 42.6
6.	ϕ^{ES} Overlap	5.789 ± 0.686	-0.329 ± 0.945	1.086 ± 0.259	0 - 27.3

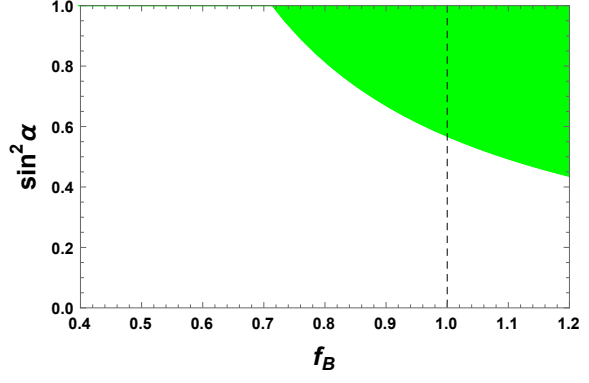
Table 6: Constraints on active and sterile neutrino in units of $10^6 \text{cm}^{-2} \text{s}^{-1}$.

4.1 The $\sin^2\alpha$ and f_B Degeneracy

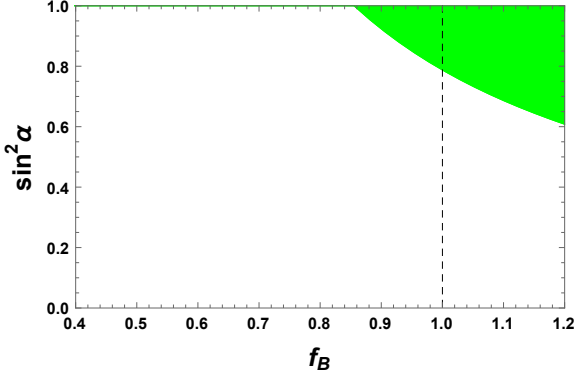
Using the equation which relates the f_B and $\sin^2\alpha$ i.e. the equation (17), we obtain $\sin^2\alpha$ - f_B degeneracy plots for all the chosen Sets. For SNO-III, $\sin^2\alpha$ varies from 61.3% to 100%. For SK Combined at $\sin^2\alpha$ varies from 43.4% to 100%. For KamLAND it varies from 60.7% to 100%. For Borexino(3MeV) and Borexino(5MeV), $\sin^2\alpha$ varies from 47% to 100% and 44.3% to 100% respectively. For ϕ^{ES} Overlap, $\sin^2\alpha$ varies from 80.6% to 100%. The constraints for active and sterile neutrinos is depicted in Table (6). The variation of f_B with $\sin^2\alpha$ for the fixed value of $\sin^2\psi$ i.e.1, obtained from the analysis is shown in the Figure (2) for different Sets.



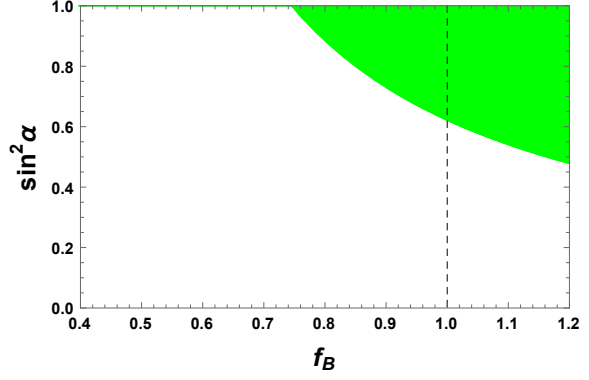
(a) f_B vs $\sin^2\alpha$ plot for SNO-III.



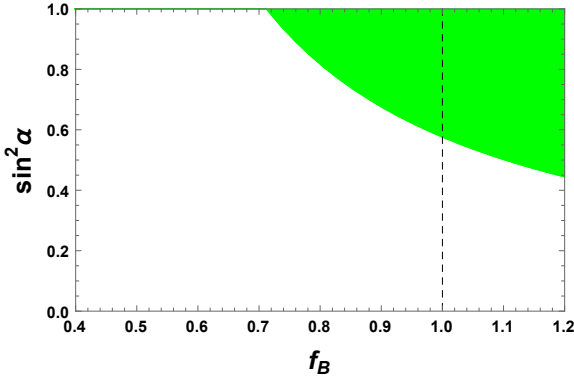
(b) f_B vs $\sin^2\alpha$ plot for SK Comb.



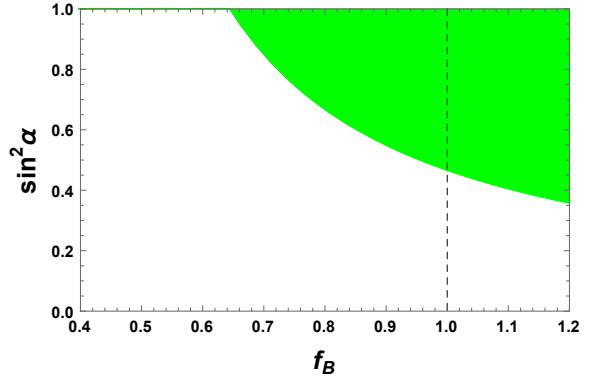
(c) f_B vs $\sin^2\alpha$ plot for KamLAND.



(d) f_B vs $\sin^2\alpha$ plot for Borexino(3MeV).



(e) f_B vs $\sin^2\alpha$ plot for Borexino(5MeV).



(f) f_B vs $\sin^2\alpha$ plot for ϕ^{ES} Overlap.

Figure 2: f_B vs $\sin^2\alpha$ common parameter space plots for all six Sets.

4.2 Medium Energy Neutrino Data Analysis

Here we use equation (19), which relates $\sin^2\alpha$ and $R_{BOR/KL}^{ES}$, and we obtain $\sin^2\alpha$ vs $R_{BOR/KL}^{ES}$ plots for different values of P_{ee} from different experiments. The values of P_{ee} for different experiments is taken from Table(2).

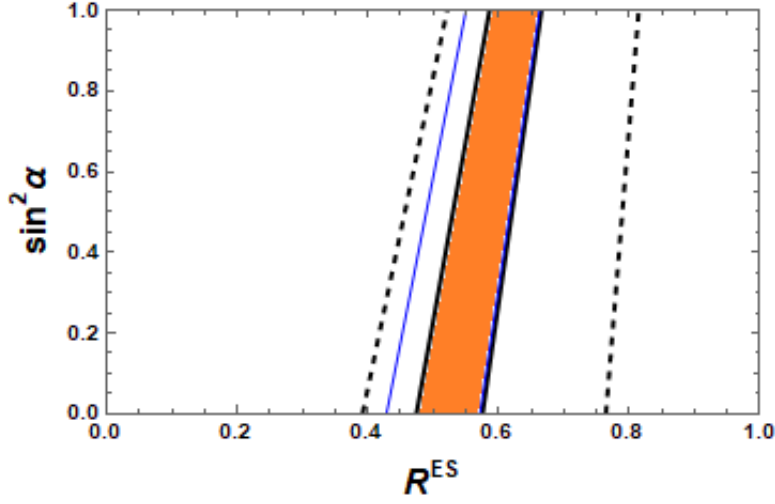


Figure 3: 1σ plot of $\sin^2\alpha$ vs R^{ES} for KamLAND(Dotted lines), Borexino Phase-I(Thin Lines) and Borexino Phase-II(Thick lines). The shaded region corresponds to the overlapping region of three experiments.

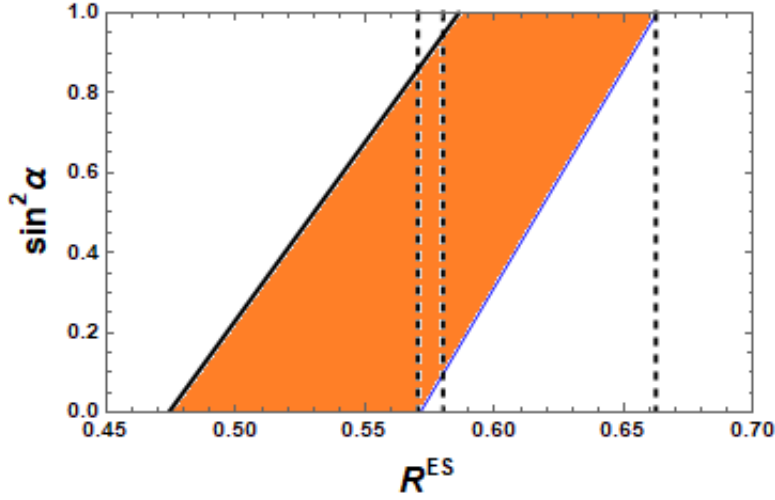


Figure 4: 1σ plot of $\sin^2\alpha$ vs R^{ES} zoomed for overlapping region of KamLAND, Borexino Phase-I and Borexino Phase-II. Vertical dotted lines corresponds to R^{ES} equal to 0.57 , 0.58 and 0.66.

We have chosen arbitrary values of R^{ES} . There is 15% sterile neutrino component in the solar neutrino flux corresponding to $R^{ES} = 0.57$ at 1σ and 6% sterile neutrino component corresponding to $R^{ES} = 0.58$ at 1σ . Here $R^{ES} = 0.66$ corresponds to no sterile component.

4.3 The χ^2 -Analysis Constraints

We classified the data in various five cases as the best possible combinations. In Case-I we have used R^{NC} , R^{CC} and R^{ES} from all experiments. In Case-II we have used experiment results with best precision. So we have used R^{NC} from SNO-II, R^{CC} from SNO-I, SNO-II, SNO-III and R^{ES} from SK-I, SK-III, SK-IV and SK Combined. In Case-III we have used R^{NC} and R^{CC} from all the SNO-I, SNO-II, SNO-III experiments and R^{ES} from all experiments except SNO-III as it has very less rate as compared to other experiments. In Case-IV we have used R^{NC} and R^{CC} from all the SNO-I, SNO-II, SNO-III experiments and R^{ES} from SNO-III only. In Case-V we have used R^{NC} and R^{CC} from all the SNO-I, SNO-II, SNO-III experiments and R^{ES} from the overlapping region of all the experiments for R^{ES} as shown in Figure (5). All these different Cases are shown in Table (7).

Case	R^{CC}	R^{NC}	R^{ES}
I	SNO-I, SNO-II, SNO-III.	SNO-I, SNO-II, SNO-III.	SNO-I, SNO-II, SNO-III, SK-I, SK-II, SK-III, SK-IV, SK Combined, KamLAND, Borexino(3MeV) and Borexino(5MeV).
II	SNO-I, SNO-II, SNO-III.	SNO-II	SK-I, SK-III, SK-IV and SK Combined.
III	SNO-I, SNO-II, SNO-III.	SNO-I, SNO-II, SNO-III.	SNO-I, SNO-II, SK-I, SK-II, SK-III, SK-IV, SK Combined, KamLAND, Borexino(3MeV) and Borexino(5MeV).
IV	SNO-I, SNO-II, SNO-III.	SNO-I, SNO-II, SNO-III.	SNO-III
V	SNO-I, SNO-II, SNO-III.	SNO-I, SNO-II, SNO-III.	R^{ES} Overlap

Table 7: Different Cases for χ^2 analysis.

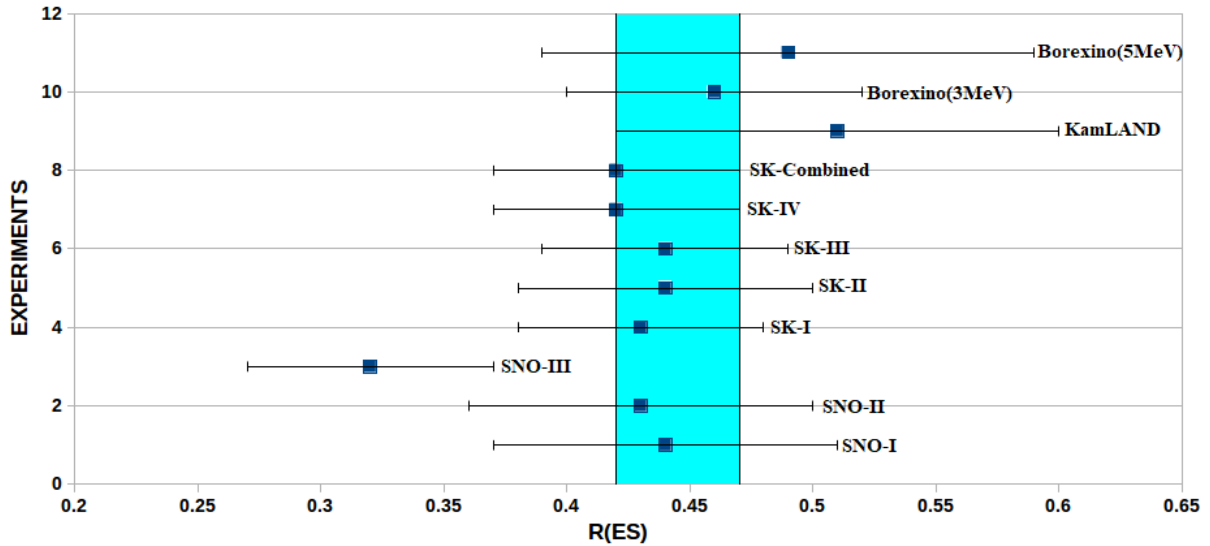


Figure 5: R^{ES} Overlap region (shaded) from all experiments.

Here we have done the χ^2 -fitting for all the various cases with all the possible degrees of freedom using the χ^2 formula given by the equation below:

$$\chi^2 = \sum_i \frac{(R_i - R_i^{th})^2}{\delta R_i^2} \quad (20)$$

The sum is extended over all the experimental data points ($i = ES_{SK}, ES_{SNO}, ES_{KL}, ES_{Bor}, NC, CC, etc.$) as depicted in Table (3). Here R_i and δR_i denote the experimental rates and their errors, and R_i^{th} are the theoretical values given by equations (14), (15) and (16). χ^2_{min}/ν shown in tables below is reduced χ^2 minimum and ν is the degrees of freedom. We have fixed the value of $\sin^2\psi$ to 1 taking no antineutrino component possibility.

No. of d.o.f.	f_B	P_{ee}	$\sin^2\alpha$	$\frac{\chi^2_{min}}{\nu}$	Sterile % (1σ)
16 d.o.f.	0.974	0.327	0.970	0.363	0-31.5
15 d.o.f.	0.975	0.327	0.970	0.387	0-31.5
14 d.o.f.	0.975	0.327	0.970	0.415	0-31.5

Table 8: Results of χ^2 analysis for Case - I

No. of d.o.f.	f_B	P_{ee}	$\sin^2\alpha$	$\frac{\chi^2_{min}}{\nu}$	Sterile % (1σ)
7 d.o.f.	0.962	0.332	0.970	0.138	0-22.5
6 d.o.f.	0.965	0.332	0.970	0.161	0-22.5
5 d.o.f.	0.965	0.332	0.970	0.194	0-22.5

Table 9: Results of χ^2 analysis for Case - II

No. of d.o.f.	f_B	P_{ee}	$\sin^2\alpha$	$\frac{\chi^2_{min}}{\nu}$	Sterile % (1σ)
15 d.o.f.	0.982	0.330	0.970	0.127	0-26.8
14 d.o.f.	0.985	0.330	0.970	0.136	0-26.8
13 d.o.f.	0.985	0.330	0.970	0.146	0-26.8

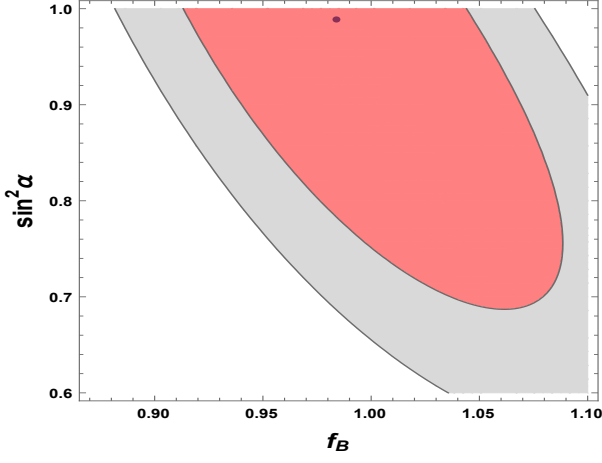
Table 10: Results of χ^2 analysis for Case - III

No. of d.o.f.	f_B	P_{ee}	$\sin^2\alpha$	$\frac{\chi^2_{min}}{\nu}$	Sterile % (1σ)
6 d.o.f.	0.921	0.322	0.970	0.441	0-19.4
5 d.o.f.	0.924	0.322	0.970	0.530	0-19.4
4 d.o.f.	0.924	0.322	0.970	0.662	0-19.4

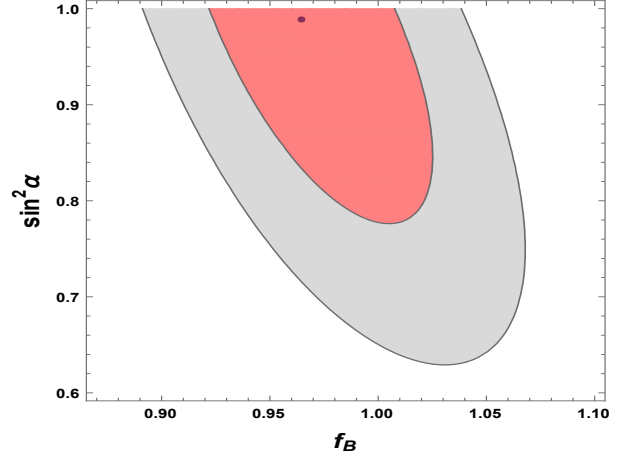
Table 11: Results of χ^2 analysis for Case - IV

No. of d.o.f.	f_B	P_{ee}	$\sin^2\alpha$	$\frac{\chi^2_{min}}{\nu}$	Sterile % (1σ)
6 d.o.f.	0.956	0.328	0.970	0.118	0-18.4
5 d.o.f.	0.957	0.328	0.970	0.141	0-18.4
4 d.o.f.	0.957	0.328	0.970	0.177	0-18.4

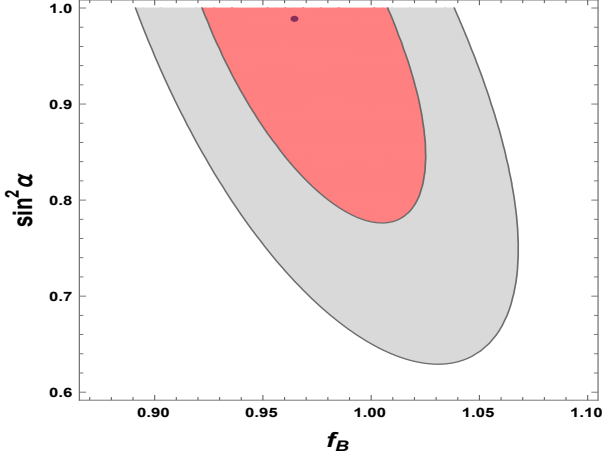
Table 12: Results of χ^2 analysis for Case - V



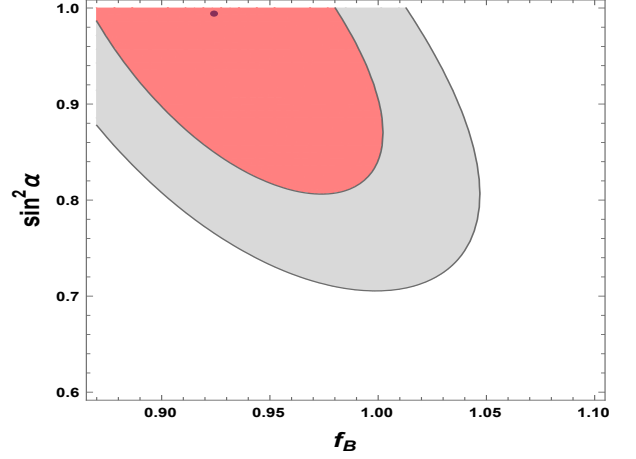
(a) 1σ , 2σ contour plots in the f_B , $\sin^2\alpha$ plane for Case-I.



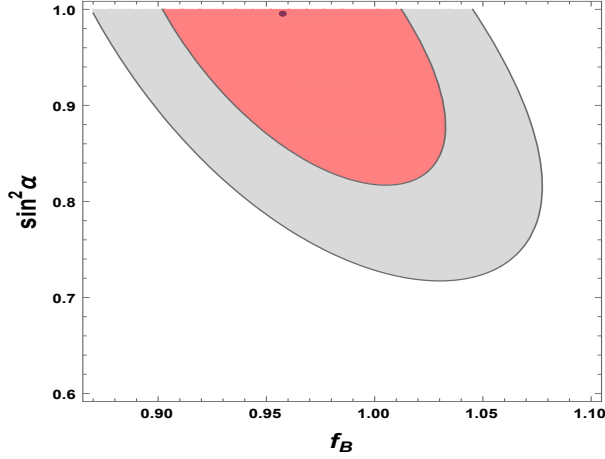
(b) 1σ , 2σ contour plots in the f_B , $\sin^2\alpha$ plane for Case-II.



(c) 1σ , 2σ contour plots in the f_B , $\sin^2\alpha$ plane for Case-III.



(d) 1σ , 2σ contour plots in the f_B , $\sin^2\alpha$ plane for Case-IV.



(e) 1σ , 2σ contour plots in the f_B , $\sin^2\alpha$ plane for Case-V.

Figure 6: 1σ , 2σ contour plots for all five Cases. The dot represents the best fit point.

As can be seen from Figure (6), we have obtained more constrained results for Case-V. For Case-V there is very less fraction of sterile component which is 18.4% at 1σ , as shown in Table (12). For Case-I, there is a possibility of 31.5% sterile fraction at 1σ . For Case-II, we have possibility of 22.5% sterile fraction at 1σ . For case-III, 1σ range for $\sin^2\alpha$ indicates possibility of 26.8% of sterile fraction. For Case-IV, we have possibility of 19.4% sterile fraction at 1σ .

5 Conclusions

The constraints on the flux of sterile neutrinos present in solar neutrino data would reveal many riddles still hidden in the solar neutrino physics, and as well as in the neutrino astrophysics as a whole. In this work, we derived such constraints in a model independent way i.e. on the flux of sterile neutrinos ν_s , which are more stringent as compared to the existing in literature. The global and comprehensive analysis of the solar neutrino data available from all the solar neutrino experiments including KamLAND solar phase and Borexino(3MeV), Borexino(5MeV) have been done. Therefore, it became interesting to check the bounds obtained by such investigation.

We calculated the upper bound on the flux of $\phi_{sterile}$ present in the solar neutrinos, i.e. the 1σ upper bounds for the $\phi_{sterile}$ are obtained for the all the cases as

$$\begin{aligned}\phi_{sterile} &\leq 0.11 \times 10^6 cm^{-2}s^{-1} \text{ (SNO-III)} \\ \phi_{sterile} &\leq 0.95 \times 10^6 cm^{-2}s^{-1} \text{ (SK Combined)} \\ \phi_{sterile} &\leq 1.93 \times 10^6 cm^{-2}s^{-1} \text{ (KamLAND)} \\ \phi_{sterile} &\leq 1.06 \times 10^6 cm^{-2}s^{-1} \text{ (Borexino(3MeV))} \\ \phi_{sterile} &\leq 1.64 \times 10^6 cm^{-2}s^{-1} \text{ (Borexino(5MeV))} \\ \phi_{sterile} &\leq 0.62 \times 10^6 cm^{-2}s^{-1} (\phi^{ES} \text{ Overlap})\end{aligned}$$

It is clear that more constrained bounds are obtained in Set-1(SNO-III). Set-6 in which we have used ϕ^{ES} Overlap is also giving very constrained bounds on sterile. It may be noted that these bounds are more constrained as compared to the ones obtained earlier in literature [17], [18], [19], [20], [21] and [26].

The column 5 of Table (6) represent the fraction of active neutrinos present in the solar neutrino flux. The 1σ range of $\sin^2 \alpha$ for KamLAND indicate strong possibility, i.e. up to 49.8%, of sterile neutrino (which is proportional to $\cos^2 \alpha$) percentage given in column 6 at 1σ range. However, in the SK Combined case there is a possibility upto 24.8% for sterile fraction at 1σ . The 1σ range of $\sin^2 \alpha$ for Borexino(3MeV) and Borexino(5MeV) indicate possibility up to 27.8% and 42.6% respectively. However, in the Set-1 there is very less possibility for sterile fraction, which is 5.6% at 1σ .

From $\sin^2 \alpha - f_B$ degeneracy plots we obtained upper limits on sterile component as

$$\begin{aligned}&\leq 38.7\% \text{ (SNO-III)} \\ &\leq 56.6\% \text{ (SK-Combined)} \\ &\leq 39.3\% \text{ (KamLAND)} \\ &\leq 53.0\% \text{ (Borexino(3MeV))} \\ &\leq 55.7\% \text{ (Borexino(5MeV))} \\ &\leq 49.6\% (\phi^{ES} \text{ Overlap})\end{aligned}$$

It is clear that most constrained limits on sterile component are obtained in Set-1 and Set-3, where we have used SNO-III and KamLAND data respectively.

From medium energy data analysis, we see that there is a possibility of no sterile component corresponding to reduced $R^{ES} = 0.66$.

Also from χ^2 analysis we obtained that there is a possibility of 31.5%, 22.5%, 26.8%, 19.4% and 18.4% sterile component for Case-I, II, III, IV and V respectively.

From all the cases discussed above, we have obtained most constrained value of sterile neutrino component in Set-1 as shown in Table(6), where we have used equation (13). It shows that there is 5.6% of sterile component in solar neutrino flux.

The indication for the existence of sterile neutrinos has emerged from WMAP data as well, which suggested that the number of neutrino families in the early universe was more than three [27]. There are several models suggested in literature, which fit the sterile neutrinos in the scheme like a 3+1 model i.e. the three ordinary neutrino and a sterile one.

The experiments like MINOS, MINOS+, LSND, MiniBooNE etc. are running and searching for the existence of sterile neutrinos. Sterile neutrinos are well motivated extensions of the SM, and symmetry protected seesaw scenarios allow for electroweak scale sterile neutrino masses and active sterile mixings. As such, the present work is quite promising for the future search of sterile neutrinos.

Acknowledgements

We acknowledge the financial support provided by the UGC, Govt. of India under the project grant MRP-MAJOR-PHYS-2013-12281. One of the authors B.C.C. thanks IUCAA for the providing hospitality during the preparation of the work.

References

- [1] R. J. Davis, D. S. Harmer and K. C. Hoffman, Phys. Rev. Lett. **20**, 1205 (1968).
- [2] B. T. Cleveland *et al.* [Homestake Collaboration], Astrophys. J. **496**, 505 (1998).
- [3] K. Eguchi *et al.* [KamLAND Collaboration], Phys. Rev. Lett. **90**, 021802 (2003).
- [4] P. Aliani, V. Antonelli, R. Ferrari, M. Picariello and E. Torrente-Lujan, arXiv:hep-ph/0406182; A.B. Balantekin, H. Yuksel, Phys.Rev. **D68**, 113002 (2003); P. Aliani, V. Antonelli, M. Picariello and E. Torrente-Lujan, New J. Phys. **5**, 2 (2003); M. Maltoni, T. Schwetz, M.A. Tortola, J.W.F. Valle, Phys.Rev. **D68**, 113010 (2003); A. Bandyopadhyay, S. Choubey, S. Goswami, S.T. Petcov, D.P. Roy, Phys. Lett. **B583**, 134 (2004); P. Aliani, V. Antonelli, M. Picariello, E. Torrente-Lujan, Phys.Rev. **D69**, 013005 (2004); P. C. de Holanda and A. Yu. Smirnov, arXiv:hep-ph/0309299; J. N. Bahcall, M. C. Gonzalez-Garcia, C. Peña-Garay, JHEP **0302**, 009 (2003).
- [5] B. C. Chauhan and J. Pulido, JHEP **0406**, 008 (2004).
- [6] A. Yu. Smirnov, Nucl. Phys. Proc. Suppl. **235**, 431 (2013); L. B. Auerbach *et al.* [LSND Collaboration], Phys. Rev. **C64**, 065501 (2001); M. Antonello *et al.*, Eur. Phys. J. **C73**, 2345 (2013); P. C. de Holanda and A. Yu. Smirnov, hep-ph/1012.5627.
- [7] P. A. Sturrock, D. O. Caldwell, J. D. Scargle, G. Walther and M. S. Wheatland, arXiv:hep-ph/0403246; P. A. Sturrock, Astrophys. J. **605**, 568 (2004); D. O. Caldwell and P. A. Sturrock, arXiv:hep-ph/0309191; P. A. Sturrock and M. A. Weber, Astrophys. J. **565**, 1366 (2002).
- [8] V. Berezhinsky, M. Narayan and F. Vissani, Nucl. Phys. **B658**, 254 (2003).
- [9] P. C. de Holanda and A. Y. Smirnov, Phys. Rev. **D69**, 113002 (2004); arXiv:hep-ph/0307266.
- [10] K. Eguchi *et al.* [KamLAND Collaboration], Phys. Rev. Lett. **92**, 071301 (2004).
- [11] B. Aharmim *et al.* [SNO Collaboration], Phys. Rev. **C87**, 015502 (2013).
- [12] B. Abharmim *et al.* [SNO Collaboration], nucl-ex/05022021; Phys. Rev. Lett. **101**, 111301 (2008).
- [13] K. Abe *et al.* [The Super-Kamiokande Collaboration], Phys. Rev. **D94**, 052010 (2016).
- [14] M. Agostini *et al.* [Borexino Collaboration], arXiv:1709.00756v1[hep-ex].
- [15] G. Bellini *et al.* [Borexino Collaboration], Phys. Rev. **D82**, 033006 (2010).
- [16] S. Abe *et al.* [The KamLAND Collaboration], Phys. Rev. **C84**, 035804 (2011).
- [17] V. D. Barger, D. Marfatia and K. Whisnant, Phys. Lett. **B509**, 19 (2001); V. D. Barger, D. Marfatia and K. Whisnant, Phys. Rev. Lett. **88**, 011302 (2002); V. Barger, D. Marfatia, K. Whisnant and B. P. Wood, Phys. Lett. **B537**, 179 (2002); A. B. Balantekin, V. Barger, D. Marfatia, S. Pakvasa and H. Yuksel, Phys. Lett. **B613**, 61 (2005).
- [18] V. Barger, *et al.* Phys. Rev. Lett. **88**, 011302 (2002); Phys. Lett. **B537**, 179 (2002); A. Bandyopadhyay, *et al.* Phys. Lett. **B540**, 14 (2002).
- [19] S. K. Kang and C. S. Kim, Phys. Lett. **B584**, 98-102 (2004).

- [20] Bhag C. Chauhan and J. Pulido, JHEP**0412**, 040 (2004).
- [21] S. Dev, Sanjeev Kumar and Surender Verma, Modern Physics Letters **A21**, 1761 (2006).
- [22] H. Nishino *et al.* Null. Instrum. Methods Pays. Res. Sect. **A 610**, 710 (2010); S. Yamada *et al.*, IEEE Trans. Nucl. Sci. **57**, 428 (2010).
- [23] A. Gando *et al.* [KamLAND Collaboration], Phys. Rev. **C92**, 055808 (2015).
- [24] Nuria Vinyoles *et al.* The Astrophysical Journal, **835**, 2 (2017).
- [25] M. Agostini *et al.* [Borexino Collaboration], arXiv:1707.09279v2[hep-ex].
- [26] Govind Singh, Ashish Sharma, Gazal Sharma, Shankita Bhardwaj, Surender Verma, B.C. Chauhan, XXII DAE-HEP Symp. Springer Proc. in Physics 203, Ch.12, 59 (2018); Lal Singh, Bhag C. Chauhan, Ravi Dutt, K. K. Sharma and S. Dev, arXiv:1102.4917v1 [hep-ph].
- [27] Komatsu *et al.* [WMAP Collaboration], Astrophys. J. Suppl., 192 (2011).